Chapter 3

Modulation of Drug Release: Exploring the Influence of Diisocyanate Variants on Polyurethane Matrix

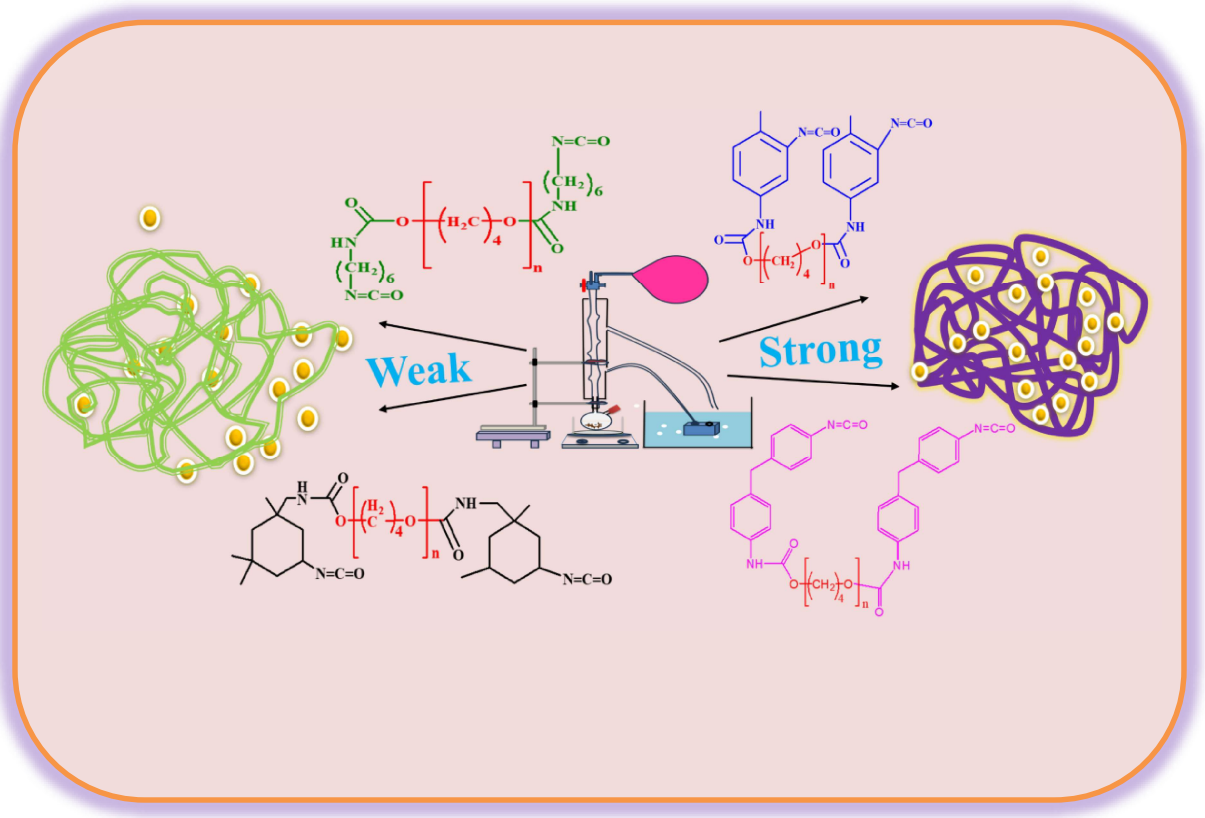

This work has been published in *ACS Applied Polymer Materials* 6.16 (2024): 9499-9511.

Chapter 3

3.1 Introduction

In this study, the adjustment of different diisocyanate segments (2,4-toluene diisocyanate, 4,4′-methylene diphenyl isocyanate, 1,6-hexamethylene diisocyanate, and isophorone diisocyanate) facilitated the achievement of unique release profiles for the hydrophobic drug PTX. Notably, PU containing aromatic diisocyanate exhibits less than 20% drug release in PBS (pH 7.4), whereas those with aliphatic diisocyanates demonstrate a release of ∼80%. From contact angle measurements, PU-I (IPDI-based PU) is found to be more hydrophilic. The combination of different diisocyanates with poly(tetramethylene glycol) influences the distribution and location of drugs within the polymer matrix, leading to diverse drug release mechanisms. Additionally, cellular adhesion experiments with SiHa cells validate the well-spread morphologies of the PU samples with greater adherence to the cell surfaces. FTIR analysis confirms the presence of the −NH– bond, which is in good agreement with the NMR spectra. These findings are discussed in detail below.

3.2 Results and Discussion

3.2.1 Structure-Property correlation in various Polyurethanes

The preparation of different diisocyanate-based polyurethanes (PUs) involves careful control of the chemical reaction between the hydroxyl group (chain end) of PTMG and different diisocyanates. The controlled reaction results in the formation of various structures are confirmed by FTIR, UV–VIS, NMR, and XRD spectroscopy, as shown in **Figure 3.2.1** The initial broad N–H peak at 3308 cm^{-1} in PU-M[124] changes to a lower wavenumber for PU-T (3290 cm^{-1}), while in PU-I and PU-H, it shifts to higher wavenumbers at 3337 and 3328 cm^{-}

[1], respectively. It is important to note that the stronger the bond, the higher the stretching frequency (**Figure 3.2.1a**). These shifts from free >N–H (appearing at around 3400–3500) confirm the presence of a hydrogen-bonded >N–H peak in all the systems[125]. The disappearance of the peak around 2270–2300 cm^{-1} (assigned to the –NCO group)[126] confirms the completion of the reaction. The out-of-plane (oop) C–H bending at 815 cm^{-1} was detected in both PU-T and PU-M and was attributed to the presence of an aromatic alkene system in these materials[127]. The >CO stretching peaks exhibit a decreasing trend in wavenumbers, going from 1731 in PU-M,1729 in PU-T, and 1723 in PU-H to 1720 cm^{-1} in PU-I[128–130]. This trend corresponds to a shift from aromatic to aliphatic structures since pi-acceptors are attached directly here. Additionally, the presence of medium-strength peaks near 1595, 1599, 1557, and 1574 cm^{-1} confirms in-plane N–H stretching[130]. Furthermore, the peaks at 1220 and 1219 cm^{-1} arise from the vibration of C═C bonds in the benzene ring present in PU-M and PU-T, respectively[131]. The peaks observed in the range of 1643–1620 cm^{-1} [132] in all PU samples; 1536, 1512, and 1414 cm^{-1} in PU-M; and 1537,1507, and 1412 cm^{-1} in PU-T can be attributed to the stretching vibrations of (H-bonded) COO^{-1} and the C–C ring, respectively[127]. These vibrations are the result of the presence of the benzene ring in the molecular structures of PU-M and PU-T moieties. The peak ranging from 1372–1364 cm^{-1} is due to the −CO–O–C– group in all samples[126]. The UV–vis spectra for all samples were analyzed within the range of 200–400 nm, as shown in **Figure 3.2.1b**. PU-M exhibits distinct absorption bands at 273 and 332 nm, which can be attributed to π–π* and n−π* transitions, respectively[133]. Notably, when comparing the UV–vis absorption peaks of polymers, a consistent shift toward shorter wavelengths is observed as we move from PU-T (263 and 306 nm) to PU-I (231 and 262 nm) and PU-H (254 and 285

nm)[134]. This shift toward the blue end of the spectrum can be attributed to the deviation of conjugation as we move from aromatic to aliphatic PU (hypsochromic shift). Furthermore, the NMR spectra conclusively demonstrate the progression of the reaction beyond the

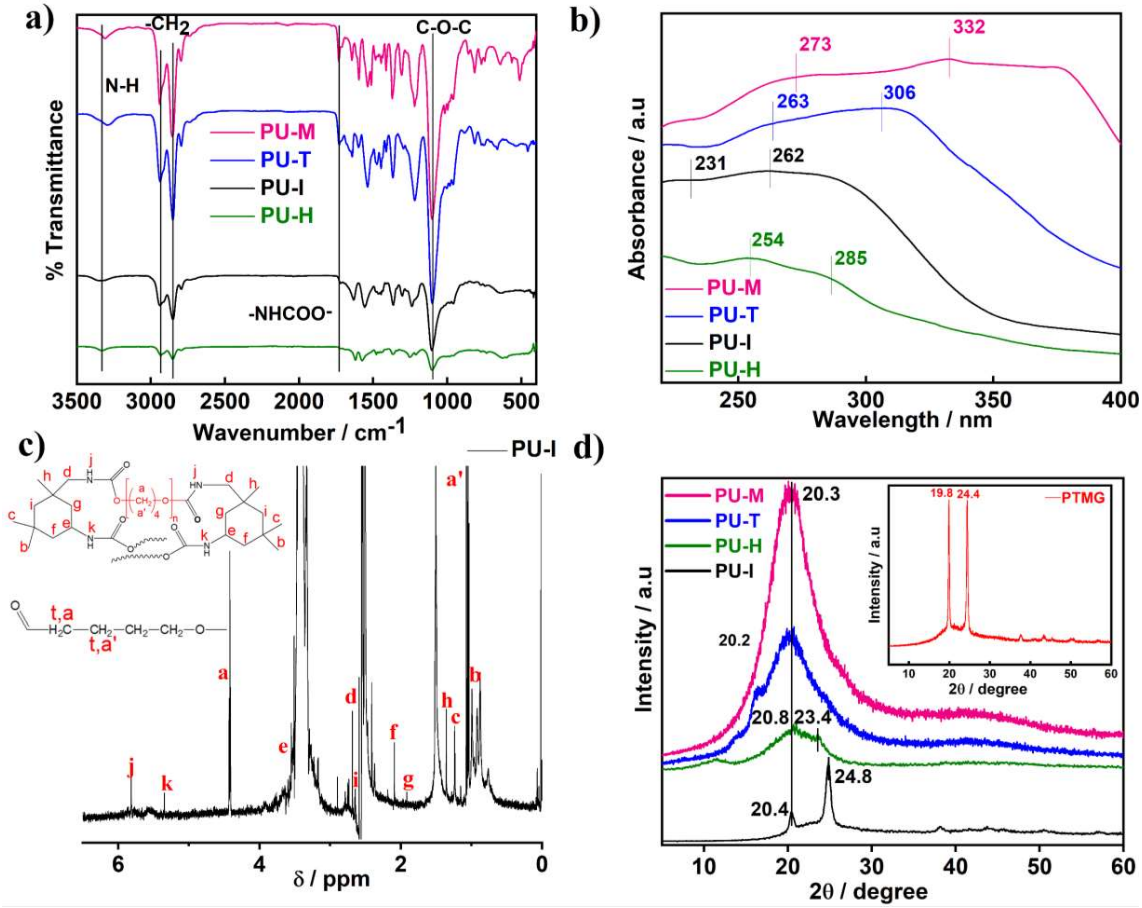

Figure 3.2.1: (a) FTIR spectra of all aromatic and aliphatic polyurethanes showing shifts in peak positions due to interactions. (b) UV–vis spectra showing peak positions for $\pi \rightarrow \pi^*$ and $n \rightarrow \pi^*$ transitions of the carbonyl peak are indicated by vertical lines. (c) ^{1}H NMR spectra of PU-I, indicating the appearance of new peaks due to polymerization; other details are provided as labeled "a", "b", etc. (d) XRD patterns of all samples showing the crystallinity; pure PTMG is shown in the inset.

prepolymer stage (**Figure 3.2.1c**). Notably, the urethane proton (−NHCOO−) exhibits signals (singlet, s) at 5.34 ppm (primary –^{s}NH–) and 5.81 ppm for secondary –^{s}NH–

[135]. Additionally, new peaks (triplet, t) are evident at 4.41[136] and 1.05 ppm, corresponding to protons of the −COO–$^{t}CH_2$– and –$^{t}CH_2$–CH2–O– groups, respectively, confirming the synthesis of polyurethane. All other peaks follow the literature-reported values[136]. It is worth mentioning that only the NMR analysis of PU-I is conducted to ascertain the NMR shifts, as it completely dissolves in d_6-DMSO, whereas others exhibit only partial solubility. XRD analysis is conducted to investigate the crystallinity of the samples utilized in this study. The results indicate that aromatic moiety-based PUs (PU-M and PU-T) exhibit an amorphous nature, showing a single diffuse peak at approximately 2θ = 23°, [135]while aliphatic moiety-based PUs show some crystallinity as evident from the extra peak at ∼23.4°. The broadening of the peak could potentially be attributed to the presence of small crystalline structures or diffraction from crystals within the PTMG material[132] (**Figure 3.2.1d**). The soft segment within the polymer derived from PTMG is of insufficient length to undergo crystallization, as evidenced by the sharp crystalline peak at 24.4°, as shown in the inset of **Figure 3.2.1d**. Furthermore, it is unlikely that diisocyanate molecules form crystalline structures in the soft segment of the polymer[137]. In the cases of PU-H and PU-I, additional peaks are observed at 23.48 and 24.82, which can be linked to the development of crystalline structures within the soft segments[138]. Given that the soft segment of the PTMG-based polymer cannot crystallize in aromatic polyurethanes due to its irregular structure and in the presence of a benzene ring in the main chain restricts itself to crystallize, aliphatic diisocyanates (HDI and IPDI) allow the soft segment to crystallize.

3.2.2 Morphological investigation

The surface morphologies of all prepolymers are examined using SEM. The SEM images

presented in **Figure 3.2.2** (**i**) depicts a smooth, uniform, and continuous surface, indicating homogeneous blending of the soft and hard segments in the case of aromatic PU[139]. The images show a distinct continuous phase formed by the amorphous soft phase, termed the matrix. Notably, a well-defined biphasic structure is prominently evident in these images for aliphatic PU (PU-H and PU-I) due to nonuniform structures of amorphous and crystalline zones[140–142].

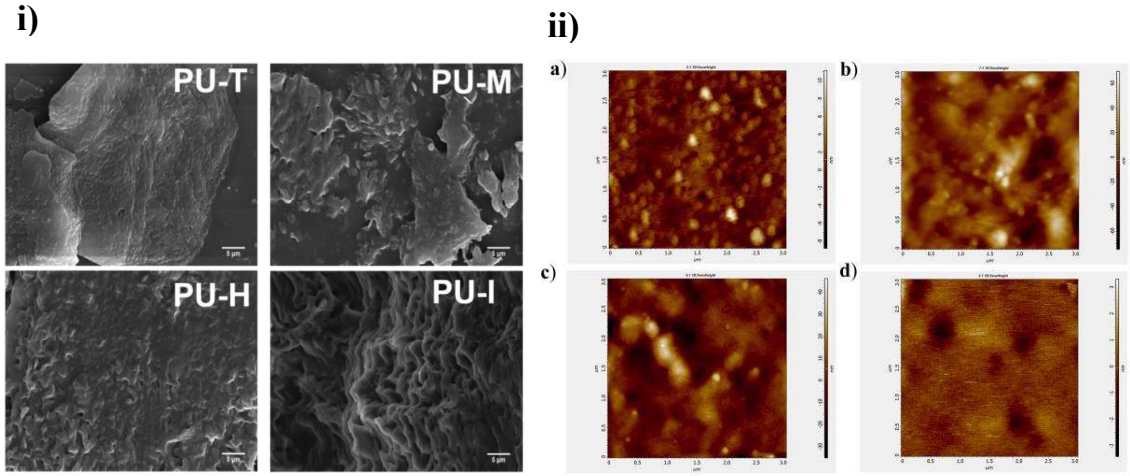

Figure 3.2.2: (i). SEM images of different PU samples (image scale: 5 μm). (ii) AFM images of (a) PU-T, (b) PU-M, (c) PU-H, and (d) PU-I in semi-contact mode (image scale for all micrographs: 3 × 3 μm^2).

Various phases containing different components developed and were observed on the fracture surfaces in this particular case. As the aromatic counterpart attached to the system increases, the sheet's cross-section becomes more uniform, suggesting that the presence of the –NCO unit significantly contributes to enhancing compatibility among the systems. AFM imaging proves effective in revealing the surface topography of polymeric films, including their roughness and the average size of their irregularities, as shown in **Figure 3.2.2** (**ii**). In PU-I, a granular morphology is observed, with its intensity notably increasing in PU-T, likely

due to the agglomeration of hydrogen-bonded structures within the hard segmented zone, as previously discussed[143,144]. The presence of larger counterparts (probably because of the vigorous reaction forming a less ordered structure) in PU-T is attributed to the intermolecular hydrogen bonding among the hard segments. The alternating bright and dark strip patterns of the domains result from hydrogen-bonded interactions between adjacent bonds, which contribute to the gradual morphological changes within the PU structure. These images depict the distinct phase separation between the two regions.

3.2.3 Mechanical and Thermal responses

The stress-strain curve obtained from the universal testing machine is depicted in **Figure 3.2.3**. **(i)a**, and the corresponding modulus and toughness values are summarized in **Table 3.2.3.1.** The molecular configuration of diisocyanate significantly affects the mechanical properties of PUs. When these polymers are stretched, they exhibit characteristics of both yield and plastic deformation along with elastic behavior. The gradual increase in the elastic

Table 3.2.3.1: Mechanical properties of PUs measured using UTM

Composition	**Elastic Modulus (MPa)**	**Tensile Strength (MPa)**	**Toughness ($KJ.m^{-3}$)**
PU-T	18.19	7.33	11359.6
PU-M	21.6	4.9	12106.5
PU-H	7.70	4.85	17985.1

modulus (Young's modulus) from aliphatic PU to aromatic is accompanied by a decrease in elongation at break. This phenomenon may be attributed to the adherence of diisocyanate to the polymer matrix, thereby stiffening the PU chain and increasing its resistance to stretching under strain. The predominant amorphous nature of aromatic PU contributes to decreased flexibility and increased shape retention. The pronounced aromatic nature of diisocyanate renders it well suited for both PU-T and PU-M, fostering vigorous reaction and reinforcing polymer structure arising from rigid aromatic rings, whereas the linear structure of HDI results in moderate crystallization behavior[145]. Owing to the benzene ring and restricted mobility of hard segments, PU-T displays the highest tensile strength (7.33 MPa), whereas weaker steric hindrance leads to a more flexible structure in PU-M compared to PU-T[146,147].The crystalline regions of the hard segment act as physical cross-linking points, contributing to the polymer's highest toughness (1798.5 kJ m^{-3}) in PU-H. In contrast, aliphatic PU leads to the formation of a more ordered structure, and this heightened orderliness in aliphatic PU contributes to its increased flexibility and toughness. Polyurethane with a higher content of soft segments is generally more flexible and elastic, which can enhance its ability to swell when in contact with biological fluids, facilitating faster drug release due to increased water uptake and diffusion pathways. The incorporation of hard segments increases the tensile strength of polyurethane, creating more rigid and less permeable regions in the polymer matrix, which leads to slower release rates as it limits the diffusion of drug molecules.

The DSC thermograms of all specimens were measured and found to be well corroborated with the reported literature[148–150]. The melting peak in the range of 15–23 °C for all PUs confirms the crystallization of the soft segment/PTMG, while the lowest melting and heat of

fusion of PU-T indicate greater interaction, which leads to a lowering of the melting temperature and heat of fusion (**Figure 3.2.3.(i)b**). Another important point that needs to be mentioned here is that PTMG is not sufficiently crystalline to form large crystalline zones. The polymer might possess a low degree of crystallinity. DSC is sensitive enough to detect small amounts of crystalline regions by showing a melting transition; however, these crystalline regions might be too small or too dispersed to form detectable diffraction patterns in XRD, which are more sensitive to long-range order. Another possibility is that these regions are highly oriented or constrained within an amorphous matrix; they might not contribute strongly to the XRD patterns[151]. Crystallinity refers to the degree of orderliness in the arrangement of the polymer chains. Crystalline regions will appear as ordered and regular, whereas amorphous regions appear more disordered and random. This is proven by the optical images (**Figure 3.2.3. (i)d**), where the crystalline regions appeared as bright[151,152], well-defined areas (PU-H and PU-I) similar to crystals in the lattice structure; in contrast, amorphous regions appeared as less distinct and more defused, as observed in PU-T and PU-M. The thermal stability of all samples is assessed using TGA and DTGA (**Figure 3.2.3. (i)c**). Degradation in an inert atmosphere is determined based on the temperature at which a 5% weight loss occurred in the sample. As depicted in the TGA curve, all of the prepared PU samples demonstrate stability up to 250 °C, with no significant degradation noted below this temperature. On the other hand, the degradation temperature is higher (327 °C) for PU-M than PU-T (253 °C), indicating better shielding of heat in the polymer matrix because of a greater number of biphenyl moieties[139,145,153,154]. All of the PU samples degrade in two steps, whereas for (aliphatic) PU-H, a single-step degradation is observed merely because of its lower molecular weight[155]. Accordingly, the thermal stability

order of structurally different diisocyanates is as follows: aryl-NCO/aryl–OH < alkyl-NCO/aryl–OH < aryl-NCO/alkyl–OH < alky-CO/alkyl–OH[156]. The aliphatic PU leads to a more ordered structure than aromatic PU, as the polymerization reaction occurs slowly for the former due to its less reactivity[152].

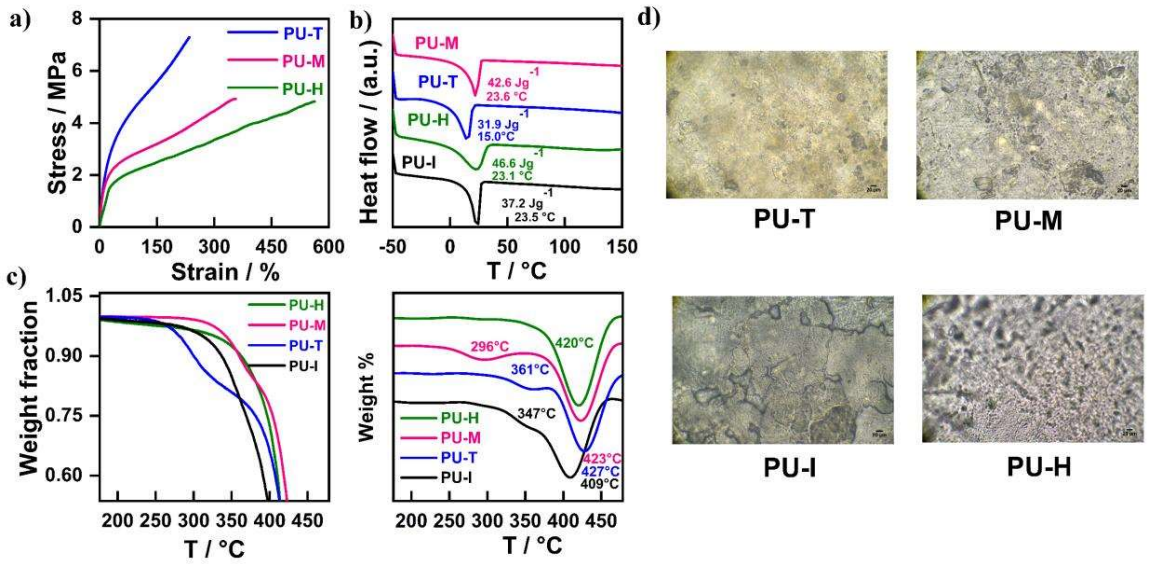

Figure 3.2.3.(i): (a) Stress-strain curves of all samples showing elongation at break, and the corresponding modulus, tensile strength, and toughness values of the polymers are compared in Table 3.2.3 (b) DSC thermograms of different PUs are shown along with the melting temperatures and heat of fusions in the corresponding color code. (c) Thermal stability (TGA thermograms and DTGA) of all PU samples, measured using a thermogravimetric analyzer. (d) Optical images of all specimens were captured at a resolution of 40×.

Aromatic isocyanates lead to polyurethanes with a more rigid structure since the benzene ring contributes to increased chemical and thermal resistance, making it more robust against degradation processes occurring at higher temperatures. Thermal degradation of PU occurs as a result of the cleavage of chemical bonds within the macromolecular chains, at the first decomposition of urethane linkages, followed by decomposition of a soft segment. The

particle size and the GPC data were calculated and provided in **Figure 3.2.3. (ii)** with the corresponding molecular weights listed in **Table 3.2.2.3.**

Table 3.2.3.2: The molecular weight of PU-I and PU-H

	Retention Time	Mn	Mw	Mp	Mz	Polydiversity
1. PU-I	16.715	6583	6684	6278	6799	1.015
2. PU-H	14.575	16526	16563	16225	16600	1.002

The small sizes of PU-I and PU-H allow for easier navigation through biological barriers and can be engineered for targeted delivery to specific cells or tissues, reducing side effects and improving therapeutic efficacy.

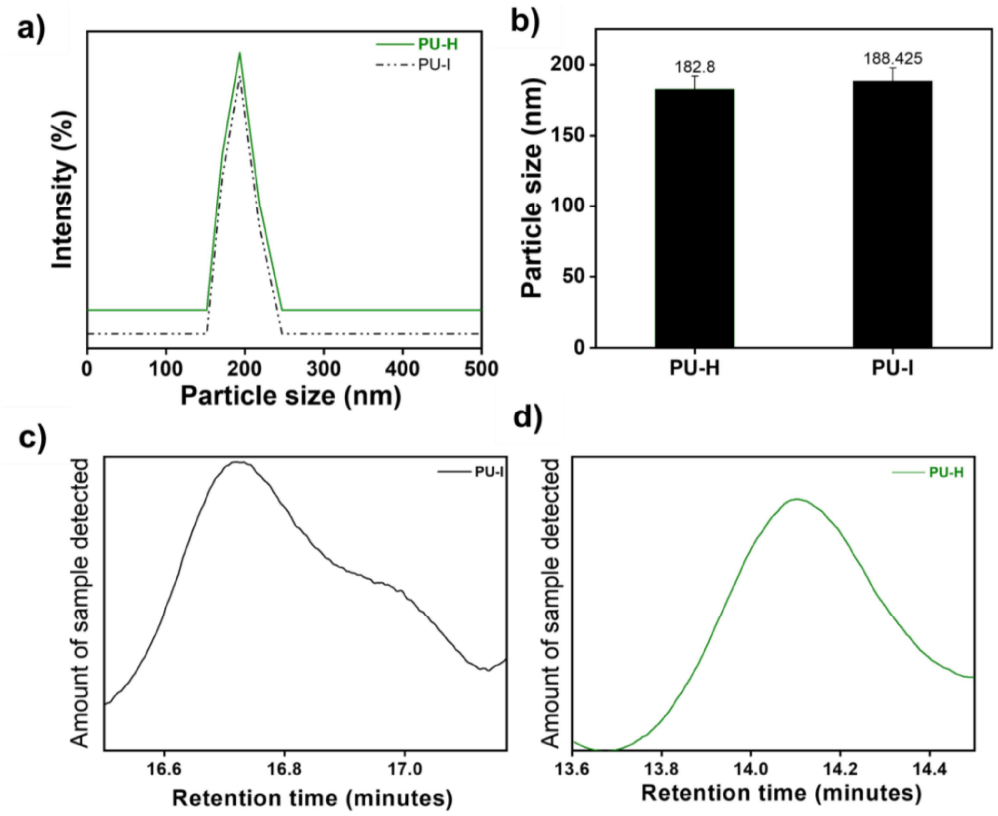

Figure: 3.2.3.(ii): Particle size analysis of polyurethane samples a) PU-I and b) PU-H are shown below, and Molecular weight determination of the polymers a) PU-I and b) PU-H that are soluble in DMF, and the corresponding data values are tabulated in Table 3.2.3.2

3.2.4 Varying Drug Release from the PU structure

To achieve controlled release, the concept of designing vehicles comes into play; here, we embedded guest biological molecules (anticancer drug paclitaxel)[157] within the PU matrices. PU-T, PU-M, PU-H, and PU-I show releases of 7, 17, 28, and 40% in 24 h, respectively (**Figure 3.2.4.i.a**). Monitoring the release pattern of paclitaxel in the PBS buffer solution over time reveals a steady and sustained release from crystalline PUs (PU-I and PU-H), while

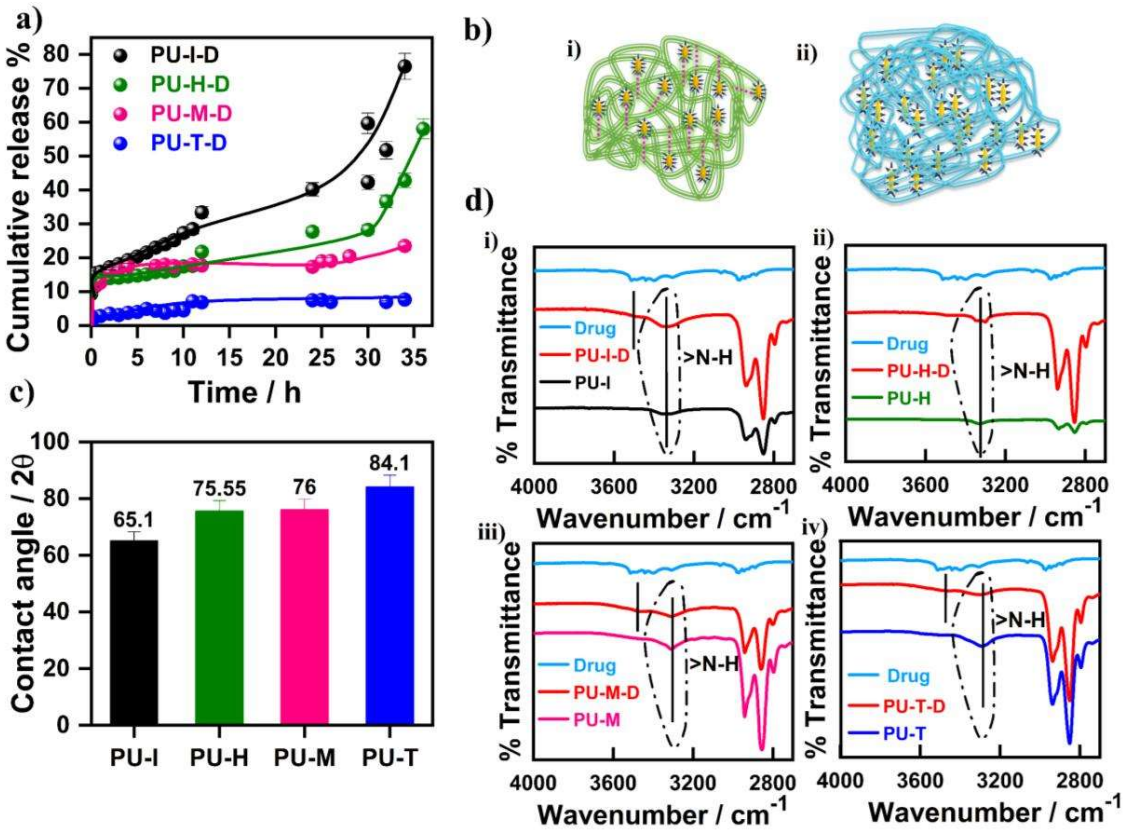

Figure 3.2.4.i: (a) Cumulative drug release from the specimens showing sustained drug release profile from the polymers. (b) Schematic model showing the architecture of different PUs loaded with a drug that causes sustained release due to strong and weak interactions with the drug; the pink dashed lines show interactions between the drug and polymer restricting its release profile. (c) Bar diagram of the contact angle of various PUs showing polymer transition from hydrophobic to hydrophilic. (d) FTIR spectra of samples showing

polymer–drug interaction. Vertical lines indicate the respective peak position shifts due to hydrogen bonding interactions; the corresponding comparison is also shown in Table 3.2.4.1.

a relatively slow release is observed from amorphous PUs (PU-T and PU-M). This can be attributed to the strong interactions between the drug and polymer, as well as the barrier effect of the prepolymer, as confirmed through FTIR (**Table 3.2.4.1**).

Table 3.2.4.1: Comparison of FTIR Peaks and deviation from Pristine PU showing interactions

Sample	FTIR (wavenumber in cm^{-1})		Difference
	PU	PU + drug	
PU-I	3334	3334	0
PU-H	3330	3300	0
PU-M	3310	3308	2
PU-T	3290	3308	18

One important point is that the drug release kinetics of PU-H and PU-I were verified thoroughly regarding the sudden jump in the release profile, data up to 4 days were taken, and broken pieces of samples were found, presumably due to degradation. High crystallinity implies more ordered and tightly packed polymer chains, which restrict drug diffusion. This typically results in slower drug release, as the drug molecules must navigate through or around these dense crystalline regions. However, other factors like drug-polymer interactions, hydrophilicity, and branching of the polymer structure contribute to the overall drug release. The drug release profile schematically shown in **Figure 3.2.4.i.b**(i),(ii) illustrates slow and sustained release from the PU matrix (PU-T and PU-M), as opposed to

the relatively quick and greater release from PU-I and PU-H, respectively[158–160]. The drug release kinetics are further elucidated using different models, such as zero-order, first-order, Korsmeyer–Peppas, and Higuchi models, as shown in **Figure 3.2.4.ii**, and the parameters are listed in **Table 3.2.4.2**.

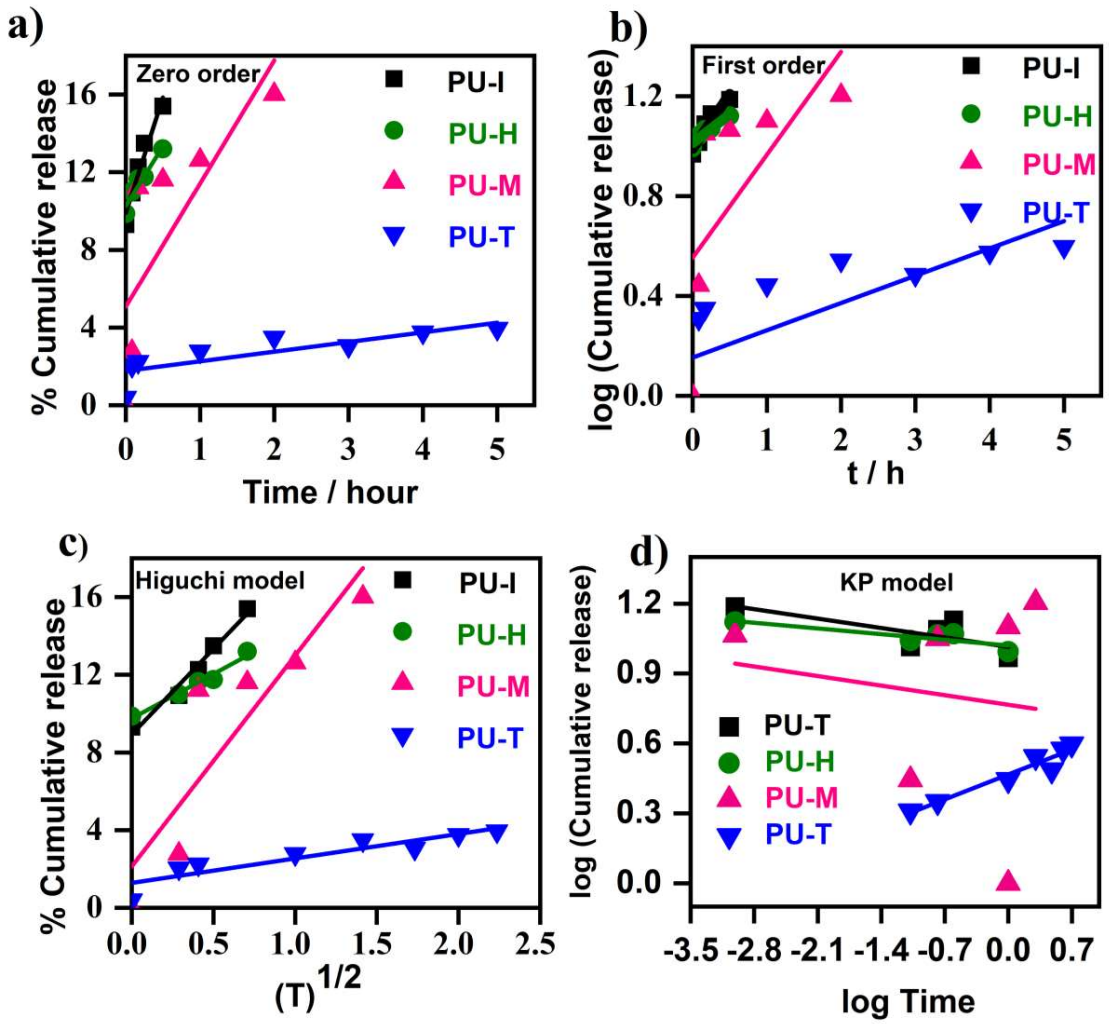

Figure 3.2.4. ii: Drug release profiles of all of the specimens with the corresponding values reported in Table 3.2.4.2.

It is evident from the figure that PU-T follows the Korsmeyer–Peppas model (KP), whereas other systems follow the Higuchi model, suggesting a non-Fickian mode of release from the

strongly interactive systems, with slow diffusion as the rate-determining step, including processes like solvent penetration into vehicles, drug dissolution, and diffusion of the drug[161]. The anomaly is well illustrated by the contact angle measurement data[127]. PU-I shows the lowest contact angle (65.1°)[162], while PU-T shows a maximum contact angle of 84.1°, as shown in **Figure 3.2.4.i.c.**

Table 3.2.4.2: The parameters of drug release profiles using various PUs

Compositions	Zero-order	First order	Higuchi model	Korsmeyer-Peppas model
PU-T	Slope =0.49±0.14 Intercept=1.76±0.36 r^2=0.68	Slope = 0.11±0.053 Intercept=0.15±0.14 r^2 =0.41	Slope =1.26±0.23 Intercept=1.28±0.32 r^2 =0.83	Slope=0.15±0.018 Intercept=0.47±0.01 r^2 =0.93
PU-M	Slope =6.34±2.51 Intercept=5.08±2.37 r^2=0.61	Slope =0.41±0.24 Intercept=0.55±0.02 r^2=0.43	Slope =10.86±2.68 Intercept=2.13±2.12 r^2=0.80	Slope =-0.06±0.19 Intercept=0.77±0.26 r^2=0.02
PU-H	Slope =6.14±0.89 Intercept=10.26±0.24 r^2=0.94	Slope =0.23±0.04 Intercept=1.012±0.01 r^2=0.91	Slope =4.58±0.42 Intercept=9.75±0.19 r^2=0.98	Slope =-0.035±0.011 Intercept=1.02±0. 017 r^2=0.75
PU-I	Slope =11.87±1.56 Intercept=9.90±0.41 r^2=0.95	Slope =0.44±0.078 Intercept=0.99±0.02 r^2=0.91	Slope =8.79±0.83 Intercept=8.93±0.373 r^2=0.97	Slope =-0.057±0.029 Intercept=1.01±0.043 r^2=0.56

Hydrophobic polyurethanes (PU-T and PU-M) exhibit lower absorption of body fluids or water, leading to inhibition of drug release from the matrix in comparison to their hydrophilic counterparts (PU-H and PU-I), likely due to the modification of the polymeric surface by the diisocyanate[163]. Contact angle is generally measured between a water droplet and a solid surface. The hydrophilic PU surfaces enhance water uptake and facilitate swelling of the polymer matrix[106], creating aqueous channels that help the drug dissolve and diffuse. This

promotes faster drug release due to increased water penetration. The dominance of the −NH– group after reaction completion at the chain end makes the polymer hydrophilic, with strong intermolecular hydrogen bonding between the chains, which is disrupted upon completion of the reaction, leading to a stronger interaction with the drug moiety and preventing drug exposure to the solvent (illustrated in **Figure 3.2.4.i.b**, strong interaction (i) and weak interaction (ii) with the drug). Moreover, the strong interaction between the drug and vehicle can be understood by thoroughly observing the FTIR measurements (**Figure 3.2.4.i.d**) of drug-loaded polymers in comparison with those of the pristine polymers. The findings from FTIR data indicate a noticeable effect on the stretching vibration of N–H in both PU–drug complexes (PU-T, PU-M), with a narrowing of the peak due to the presence of H-bonding. The H-bonding free band at 3450 cm-^{1} (for -OH group) is coming from PTX, as in pristine PU-T, no such band is there, but in pure drug, it has -OH group around 3441 cm^{-1}. A non-classical[164] or weak hydrogen bonding interaction is indicated by the blue shift of the -NH- stretching vibration from 3290 cm^{-1} to 3308 cm^{-1} upon interaction between PU-T and drug. Due to bond elongation and weakening, the stretching frequency shifts to lower wavenumbers in typical hydrogen bonding conditions. But in some other conditions, a blue shift can occur, indicating a different kind of interaction[165]. Drugs may interfere with the pre-existing H-bonding in the PU-T, decreasing overall H-bonding and frequency. Increased rigidity due to PTX binding might reinforce the N-H bond and enhance frequency of its stretching. Blue shift may be caused by enhanced N-H bond strength due to drug having electron-withdrawing groups near the interaction site. PU-T is likely to contain hydrophobic regions, and PTX is also very hydrophobic, so it will be able to bind these areas through van der Waals forces and hydrophobic bonding, which are non-covalent but still

strong enough to hold the drug. While FTIR evidence indicates a lack of strong conventional H-bonding between PTX and PU-T, the resultant slow release is explained by a combination of physical entrapment, hydrophobic interactions, diffusion restrictions, and polymer matrix effects. Such mechanisms can effectively trap the drug and regulate its release rate even without strong chemical bonding. Therefore, hydrophobicity and stronger interaction with the drug in PU-T result in almost negligible drug release in a PBS medium. However, PU-M, PU-H, and PU-I are hydrophilic and weakly interact with the drug, making these systems better carriers in terms of greater release in a sustainable manner.

3.2.5 Biocompatibility and *in-vitro* treatment efficacy

In addition to controlled drug release, an effective drug carrier must possess inherent biocompatibility for real applications in the biomedical field. Biocompatibility assessment was conducted through cell adhesion by capturing phase-contrast images of SiHa cells cultured on the materials, demonstrating enhanced cell adhesion on the PU structure, as evidenced by the well-spread morphology of all the systems (**Figure 3.2.5a**). Diisocyanates are considered toxic; however, after complete polymerization, they are converted into $-NH_2$ groups[162]. Amine groups are generally more biocompatible and participate in hydrogen bonding and other interactions with cellular proteins and extracellular matrix components[166], promoting better cellular adhesion. Amines are comparatively less reactive than isocyanate groups[167], reducing their potential for cytotoxicity, and amines can modify the surface energy of the material, making it more favorable for cell attachment. Thus, the synthesized PU samples demonstrate excellent biocompatibility, facilitating robust cell growth on their surfaces (OD values in **Figure 3.2.5b** compared to the control). Furthermore, the biological responses of all of the PU samples are evaluated through MTT assay on SiHa

cell lines for three consecutive days, revealing that PU-I exhibits superior biocompatibility over others (**Figure 3.2.5.1. (i)**; the corresponding AOPI stained images are in **Figure 3.2.5.1 (ii)**, which is also in accordance with the literature report.[162]

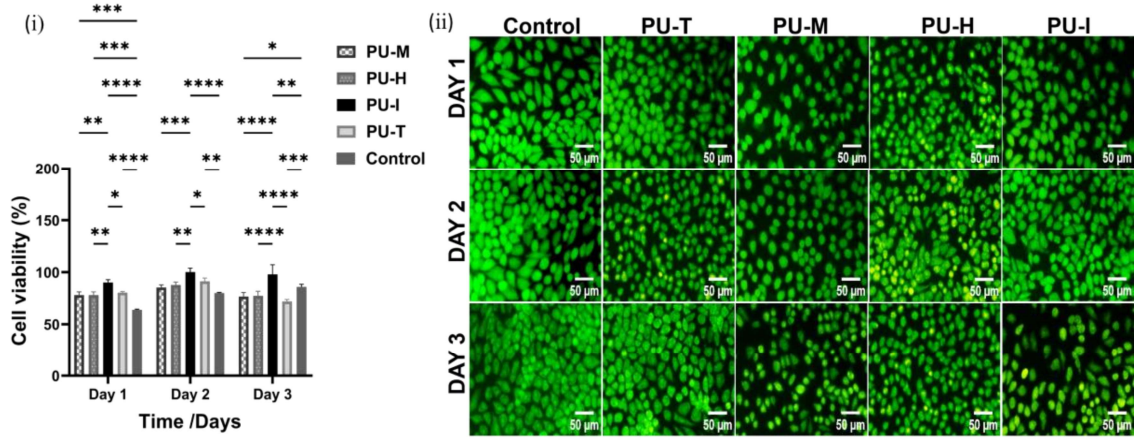

Figure: 3.2.5.1: (i) Cell viability of the materials after a study of three consecutive days. (ii)The AOPI imaging correlates with the MTT assay data, showing PU-I has better cell health and density than the other three after three consecutive days of study.

It is now pertinent to analyze the efficacy of sustained release from the PU matrix with paclitaxel-induced cell killing. Pure drug administration shows a trend of increasing cell viability (reduced cell mortality) over an extended period, despite slightly higher cell-killing efficiency observed on day 1 (**Figure 3.2.5c**). The sequence of cell-killing efficiency follows the order PU-I > PU-H > PU-M > PU-T. However, PU-I shows 55% cell viability in 3 days, and PU-T, with an identical drug concentration, exhibits 76% cell viability within a comparable time frame. Note that pure paclitaxel showed ~88% cell viability in 3 days, although the initial cell killing on day 1 is sufficiently high, at ~50%, arising from the burst release of the drug. Hence, immediate exposure to the pure drug can trigger higher cell death, while sustained release from all types of PUs can result in prolonged cell killing and achieve

higher efficiency when integrated into a drug-loaded matrix, mainly due to the sustain

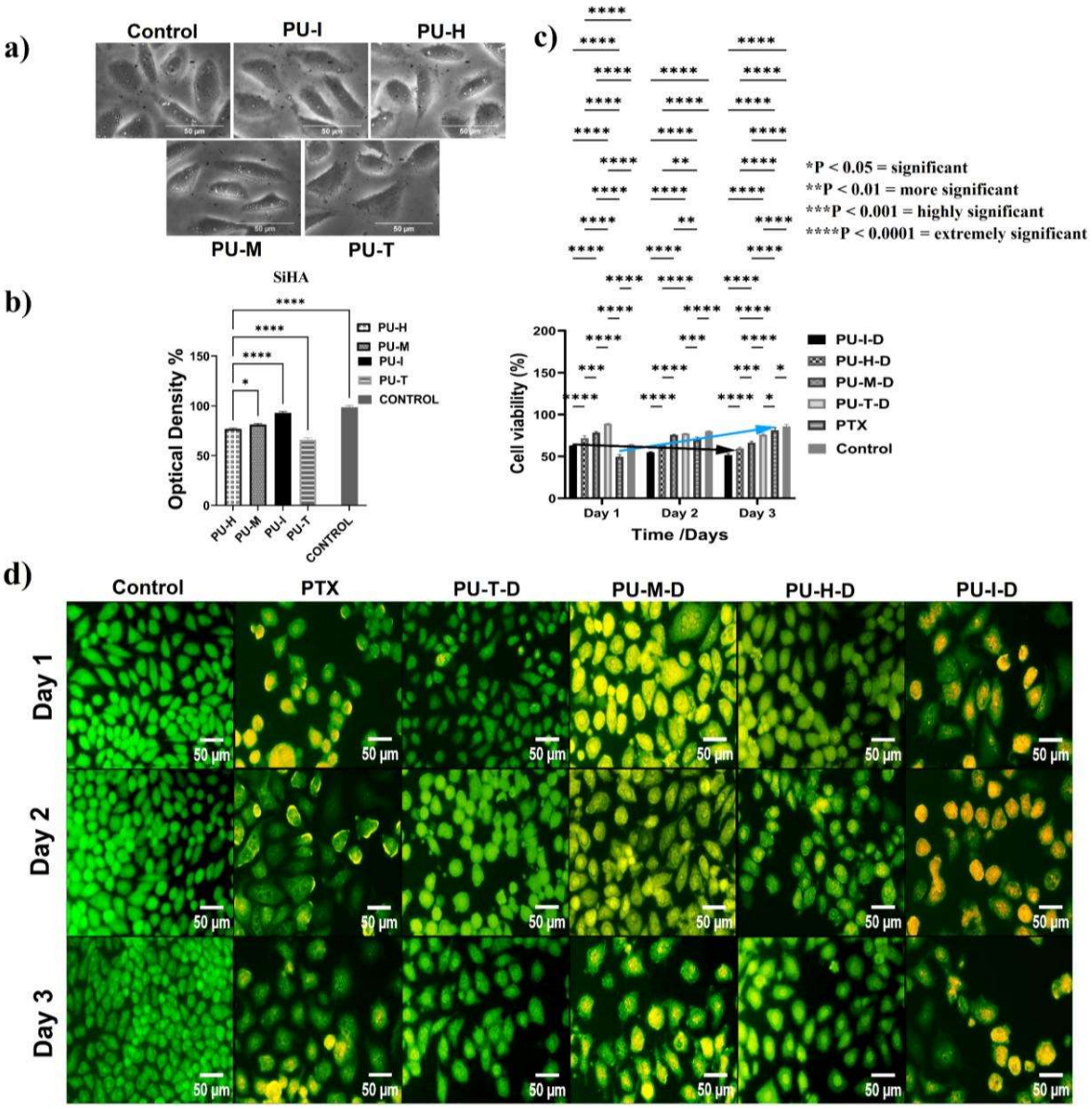

Figure 3.2.5: Biological responses of all of the polymers through cellular studies. (a) Morphology of cells grown on different PU surfaces as captured by microscopy on a gray filter after 1 day of sample proliferation (cell adhesion magnification: 40×). (b) Assessment of cell adhesion through optical density profile data of adhered cells on the sample. (c) In vitro cytotoxicity of pure drug and drug-loaded polyurethane against SiHa cells at different time intervals via MTT assay. (d) Fluorescence images after AO/EB staining of cells treated with pure drug and drug-loaded polymers, as mentioned.

release of the drug from the PU matrix[148].

It is worth mentioning that the limited availability of the pure drug over time leads to an inability to maintain the required concentration for toxicity, thereby hampering sustained cell-killing efficiency. Instead, cell proliferation persists, resulting in higher cell viability with the pure drug over an extended period. Another factor to mention here is that fast-release systems show toxicity as they quickly release a high dose to achieve therapeutic levels. Here, the drug is metabolized and cleared fast, which reduces the duration of exposure or accumulation[168]. To gain insight into the mechanism of cell killing or induced apoptosis by drug-loaded vehicles/pure drugs, we visualized SiHa cells using fluorescent imaging after staining with acridine orange (AO) and propidium iodide (PI). This dual-staining technique helps distinguish between normal and apoptotic cells based on cell membrane permeability. AO, which is permeable to the cell membrane, binds to DNA and emits green fluorescence, while PI produces red fluorescence. Generally, dead cells allow AO and PI to appear red, whereas healthy cells only allow AO to appear green. Cells stained with AO/PI exhibit an orange-yellow shade, indicating apoptosis or early necrosis, with red fluorescence indicating compromised membrane integrity, while normal healthy cells fluoresce green. In the cell line treated with drug-loaded PU-I, reduced cell density and predominantly apoptotic nature were observed, whereas cells remained viable on day 3 in the cell line treated with the pure drug (**Figure 3.2.5d**), consistent with the overall findings from the MTT assay. Thus, the impact of sustained release is markedly evident in cellular studies, highlighting the effectiveness of the carrier as a superior delivery vehicle supported by a plausible mechanism.

3.3 Conclusions

Various polyurethanes have been synthesized using a combination of aliphatic and a

aromatic diisocyanates, resulting in a diverse range of structures, hydrophilicity, and crystallinity. Polyurethanes exhibited sufficient mechanical and thermal stability. Notably, PU-I has emerged as a standout system due to its remarkable hydrophilic nature and lesser interaction with PTX, as confirmed by contact angle and FTIR analyses. It demonstrated controlled release of up to 80% of the drug within 36 h following the Higuchi model, indicating a diffusion control process. Moreover, it exhibited significant cytotoxicity (when loaded with the anticancer drug), causing approximately 55% cell death, as observed in the MTT assay results. The variations in the release characteristics were attributed to interactions between the drug and polymer, influenced by the features of both the polyurethane structure and the drug itself, along with the balance of hydrophobicity/hydrophilicity. Moreover, the branched superstructure acts as an innovative carrier for the sustained release of anticancer drugs by creating a confined environment along with appropriate interactions and a hydrophilic–hydrophobic balance. Within the confined space, PU forms localized hydrophilic and hydrophobic regions that can interact selectively with different parts of the environment, aiding the balanced release of drugs with diverse solubility properties. The limiting factor for these polymers is their solubility, which restricts their use in the desired field, and one might be careful about a suitable choice of polymer that can enhance solubility and influence drug release.